FULL PAPER

High-Performance Red, Green, and Blue Electroluminescent Devices Based on Blue Emitters with Small Singlet–Triplet Splitting and Ambipolar Transport Property

Kai Wang, Fangchao Zhao, Chenguang Wang, Shanyong Chen, Dong Chen, Hongyu Zhang, Yu Liu, Dongge Ma, and Yue Wang**

Two coordination complex emitters as well as host materials $Be(PPI)_2$ and $Zn(PPI)_2$ (PPI = 2-(1-phenyl-1*H*-phenanthro[9,10-*d*]imidazol-2-yl)phenol) are designed, synthesized, and characterized. The incorporation of the metal atom leads to a twisted conformation and rigid molecular structure, which improve the thermal stability of $Be(PPI)_2$ and $Zn(PPI)_2$ with high T_d and T_g at around 475 and 217 °C, respectively. The introduction of the electron-donating phenol group results in the emission color shifting to the deep-blue region and the emission maximum appears at around 429 nm. This molecular design strategy ensures that the highest occupied molecular orbital (HOMO) and lowest unoccupied molecular orbital (LUMO) HOMO and LUMO of $Be(PPI)_2$ and $Zn(PPI)_2$ localize on the different moieties of the molecules. Therefore, the two complexes have an ambipolar transport property and a small singlet–triplet splitting of 0.35 eV for $Be(PPI)_2$ and 0.21 eV for $Zn(PPI)_2$. An undoped deep-blue fluorescent organic light-emitting device (OLED) that uses $Be(PPI)_2$ as emitter exhibits a maximum power efficiency of 2.5 lm W^{-1} with the CIE coordinates of (0.15, 0.09), which are very close to the National Television Standards Committee (NTSC) blue standard (CIE: 0.14, 0.08). Green and red phosphorescent OLEDs (PhOLEDs) that use $Be(PPI)_2$ and $Zn(PPI)_2$ as host materials show high performance. Highest power efficiencies of 67.5 lm W^{-1} for green PhOLEDs and 21.7 lm W^{-1} for red PhOLEDs are achieved. In addition, the $Be(PPI)_2$-based devices show low-efficiency roll-off behavior, which is attributed to the more balanced carrier-transport property of $Be(PPI)_2$.

1. Introduction

Organic light-emitting devices (OLEDs) are of current interest from both scientific and practical points of view due to their applications in the next generation of full-color flat-panel displays and solid-state lighting sources.[1] During the last two decades great progress has been made in the exploitation of OLED materials and optimization of device structure. Many new emitters with red (R),[2] green (G),[3] or blue (B)[4] emission color and hosts with good carrier-transporting properties have been developed for full-color and white OLEDs.[5] To realize high-performance full-color displays and solid-state lighting, R, G, and B emission materials, which possess strictly different molecular structures, have to be used. On the other hand, R, G, and B emitters often require different hosts to achieve highly efficient energy transfer from host to emitter.[6] Therefore, the full-color and white OLEDs were often established based on a complex material system and high-cost organic syntheses. In this sense, achieving high-performance R, G, and B electroluminescence through a simple material system with the aim to reduce the production cost of materials and simplify the manufacturing process is an important issue for OLED applications.

In principle, a deep-blue-emitting material with balanced carrier-transport characteristic and relatively high triplet energy (E_T) may be employed as host for green and red phosphorescent emitters. The high E_T enables green and red phosphors to harvest the triplet energy of the blue emitter. However, the blue fluorescent materials are usually not suitable hosts for phosphorescent OLEDs (PhOLEDs) due to their low E_T and poor carrier-transport property. Recently, Schwartz, Leo, and co-workers have proposed a concept of high-efficiency white OLEDs based on a blue emitter with small singlet–triplet splitting.[7] Based on detailed theoretical and experimental studies, they demonstrated that the singlet–triplet splitting scales with the spatial overlap of the highest occupied molecular orbital

K. Wang, C. G. Wang, S. Y. Chen, D. Chen,
Dr. H. Y. Zhang, Prof. Y. Liu, Prof. Y. Wang
State Key Laboratory of Supramolecular Structure and Materials College of Chemistry
Jilin University
Changchun 130012, P. R. China
E-mail: yuewang@jlu.edu.cn
Dr. F. C. Zhao, Prof. D. G. Ma
State Key Laboratory of Polymer Physics and Chemistry
Changchun Institute of Applied Chemistry
Chinese Academy of Sciences
Changchun 130022, P. R. China
E-mail: mdg1014@ciac.jl.cn

DOI: 10.1002/adfm.201202981

(HOMO) and lowest unoccupied molecular orbital (LUMO) wave functions Ψ_{HOMO} and Ψ_{LUMO}.[7a] On the other hand, the singlet–triplet splitting becomes smaller upon decreasing of the exchange interaction integral of Ψ_{HOMO} and Ψ_{LUMO}. Consequently, a conjugated molecule with small singlet–triplet splitting should have its HOMO and LUMO localized on different moieties of the molecule. However, the design and synthesis of blue-emitting hosts for green phosphors is still a challenge because the fluorophore must have sufficiently small singlet–triplet splitting, even though blue emitters with relatively small singlet–triplet splitting have been employed as host for white, orange, and red PhOLEDs.[8] Generally, the blue or green phosphors' hosts with high E_T exhibit emission in the near-ultraviolet region and are not suitable for use as blue emitters.[9]

Aimed at developing blue emitters that can be employed as efficient hosts for green and red phosphors, we designed and synthesized two 2-(1-phenyl-1*H*-phenanthro[9,10-*d*]imidazol-2-yl)phenol (PPI)-based beryllium and zinc complexes, $Be(PPI)_2$ and $Zn(PPI)_2$. Our previous report demonstrated that 1,2-diphenyl-1*H*-phenanthro[9,10-*d*]imidazole (DPI) exhibited near-ultraviolet emission and a certain hole-transport ability.[10] To shift the emission maximum to the visible region, the electron-donating phenol group was introduced into the molecule. The PPI ligand chelation with beryllium or zinc led to the formation of a twisted and rigid molecular structure, which could enhance the stability and carrier-transport ability of the produced metal complexes. Moreover, the introduction of the phenol group may result in HOMO and LUMO localized on different moieties of the molecules, since imidazole and phenol groups have electron-withdrawing and -donating properties, respectively. The $Be(PPI)_2$ and $Zn(PPI)_2$ complexes have not only been used as emitters to fabricate deep-blue OLEDs, but also as hosts to construct high-power-efficiency green and red PhOLEDs.

2. Results and Discussion

2.1. Synthesis and Crystal Structure

Scheme 1 outlines the synthetic procedure and molecular structures of $Be(PPI)_2$ and $Zn(PPI)_2$. The ligand was prepared according to the reported method.[10] Simple refluxing of the mixture of the ligand and metal salts in methanol with sodium hydroxide and subsequent purification by vacuum sublimation produced the target $Be(PPI)_2$ and $Zn(PPI)_2$ with moderate yields (40–49%). Both complexes were fully characterized by ^1H NMR spectroscopy, mass spectrometry, and elemental analyses. All materials used in the devices were purified by repeated temperature-gradient vacuum sublimation. The molecular structure of $Be(PPI)_2$ was further determined by single-crystal X-ray crystallographic analysis. As shown in **Figure 1**, the Be^{II} atom adopts a typical tetrahedral coordination geometry and two PPI ligands chelate with a Be^{II} atom to form a molecule with spiral-type configuration. The coordination bond lengths are 1.57 (Be−O) and 1.78 Å (Be−N), respectively, which are similar to that of the previously reported molecule bis[2-(2-hydroxyphenyl)-pyridine] beryllium ($Bepp_2$).[11a] In $Be(PPI)_2$ each ligand has a torsion

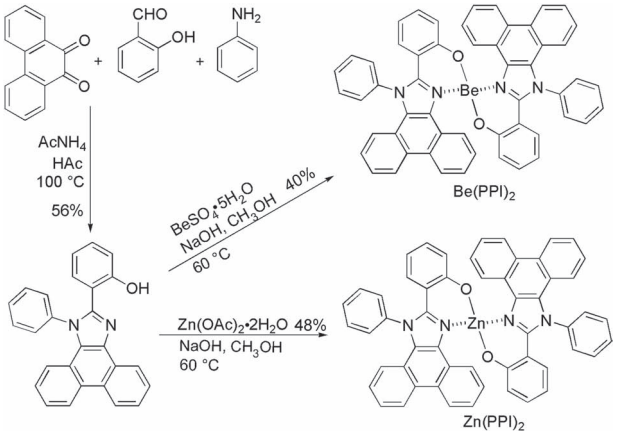

Scheme 1. Synthetic procedure and structures of $Be(PPI)_2$ and $Zn(PPI)_2$.

angle of 23° between the phenanthroimidazole plane and phenolate rings. The $Be(PPI)_2$ molecule packing in the solid state presents an intermolecular $\pi\cdots\pi$ interaction feature. Each PPI ligand of a $Be(PPI)_2$ molecule stacks together with a PPI ligand in an adjacent $Be(PPI)_2$ molecule by $\pi\cdots\pi$ interaction with a contact distance of 3.5 Å between phenanthroimidazole planes. The interaction continues on to the next molecule, which results in the formation of a one-dimensional molecular chain. Our earlier studies demonstrated that the intermolecular aromatic stacking could offer a charge-transfer pathway and enhance carrier-transport ability, which is essential for excellent electroluminescence and host materials.[11b]

2.2. Thermal Analysis

Thermal properties were investigated using thermogravimetric analysis (TGA) and differential scanning calorimetry (DSC; see Supporting Information Figure S1). Both complexes exhibited

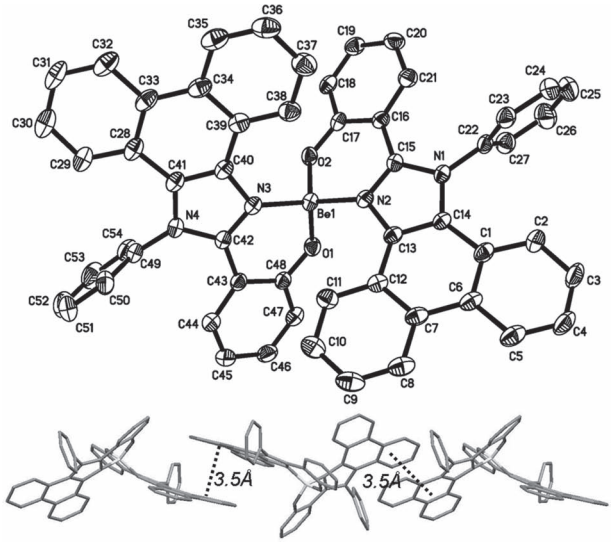

Figure 1. Molecular structure with 50% thermal ellipsoids and packing structure of $Be(PPI)_2$.

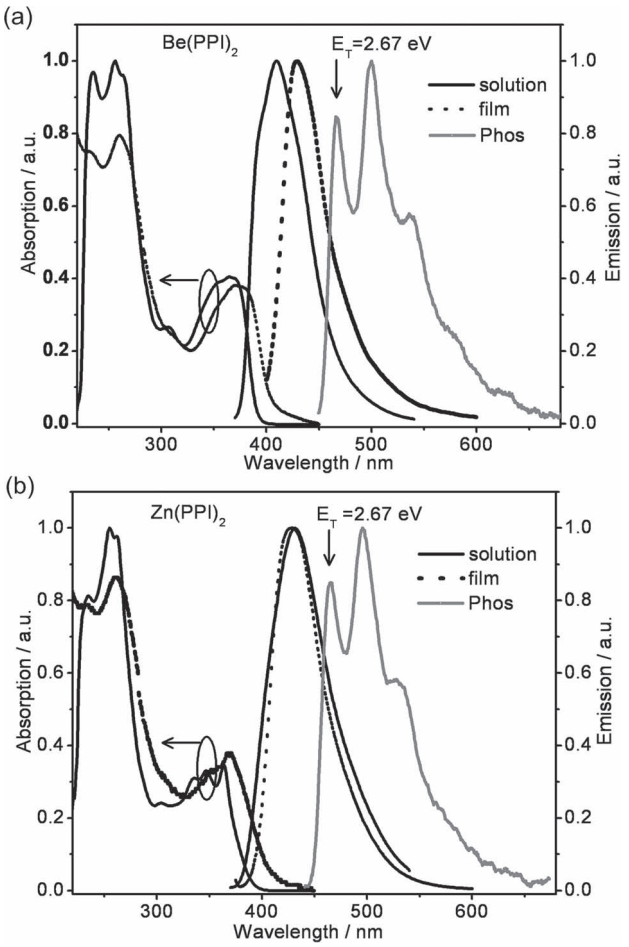

Figure 2. Room-temperature UV-vis absorption spectra, PL spectra of $Be(PPI)_2$ and $Zn(PPI)_2$ in CH_2Cl_2 solution and in neat films, as well as their phosphorescence spectra in 2-MeTHF solution (10^{-5} M) at 77 K.

good thermal stabilities as evidenced by their melting points (409 °C for $Be(PPI)_2$ and 387 °C for $Zn(PPI)_2$) and high decomposition temperatures (corresponding to 5% weight loss) of 472 °C for $Be(PPI)_2$ and 477 °C for $Zn(PPI)_2$. The glass transition temperature (T_g) of $Zn(PPI)_2$ reaches 217 °C, which is high enough for application in OLEDs and should be attributed to the rigid coordination structure. As a consequence, the excellent thermal properties of the two complexes are favorable for the formation of uniform thin films upon thermal evaporation, which are advantageous for application as lighting emitters and host materials.

2.3. Photophysical Properties

As shown in **Figure 2**, $Be(PPI)_2$ and $Zn(PPI)_2$ display similar UV-vis absorption and photoluminescence (PL) spectra. According to the absorption spectra assignment of some reported phenanthroimidazole derivatives,[4f,12] which have a similar conjugated π system to the molecules in this study, the strong absorption band peaking at approximately 260 nm can be attributed to the benzene ring. The longer-wavelength absorption bands in the range of 365 to 372 nm can be assigned to the delocalized $\pi \rightarrow \pi^*$ transition from the 2-substituted phenolate to the *N*-phenyl phenanthroimidazole ring. The two complexes exhibit intense deep-blue emissions with PL maximum at around 420 nm in both solution and vacuum-evaporated thin-film states. Their PL quantum yields (Φ_f) in solution were determined to be 0.70 for $Be(PPI)_2$ and 0.67 for $Zn(PPI)_2$, and those in film were calculated to be 0.28 for $Be(PPI)_2$ and 0.32 for $Zn(PPI)_2$. Thus, the fluorescence efficiencies of $Be(PPI)_2$ and $Zn(PPI)_2$ are comparable. It is worth noting that the full width at half maximum (FWHM) of the solid-state emission spectra are very narrow, being 48 nm for $Be(PPI)_2$ and 55 nm for $Zn(PPI)_2$. The FWHM value is very important for the color purity of deep-blue emitters. Generally, the blue emitters may have an emission maximum at around 430 nm, which is short enough for blue light. However, their emission spectra display a broad FWHM feature and extend to the longer-wavelength region, which can promote the *y* value of the CIE resulting in a sky-blue emission. The good thermal stability and small FWHMs indicate that both compounds are promising candidates for deep-blue emitters in OLEDs, although the Φ_f values in the solid state are not very high. Their triplet energies (E_T) are estimated to be 2.67 eV by the highest-energy vibronic sub-band of the phosphorescence spectra, which is sufficiently high to excite green and red phosphorescent emitters. According to the photophysical principle, E_T is the energy-level difference between the lowest vibronic level of the first excited triplet state ($T_{1,0}$) and the lowest vibronic level of the singlet ground state ($S_{0,0}$), namely, $S_{0,0} \rightarrow T_{1,0}$, which corresponds to the highest-energy phosphorescence peak. Therefore, the E_T value should be calculated from the highest-energy vibronic sub-band, which has been widely employed in the reported papers.[2b,d,6b] Similarly, the E_S implies the transition $S_{0,0} \rightarrow S_{1,0}$, which corresponds to the highest-energy fluorescence peak.[7a,9g] For both $Be(PPI)_2$ and $Zn(PPI)_2$ the singlet–triplet splitting ΔE_{ST} values are as small as 0.35 and 0.22 eV (**Table 1**), respectively, thus suggesting an energy harvesting possibility by efficient energy transfer from the triplet excited state of $Be(PPI)_2$ and $Zn(PPI)_2$ to green or red phosphorescent emitters.

Table 1. Summary of the physical properties of $Be(PPI)_2$ and $Zn(PPI)_2$.

Compound	$Be(PPI)_2$	$Zn(PPI)_2$
$T_g/T_m/T_d$ [°C]	[f]/409/472	217/387/477
λ_{abs} [nm] (sol[a]/film[b])	256,365/260,372	258,365/262,369
λ_{PL} [nm] (sol[a]/film[b])	410/429	431/429
Φ_f (sol[a]/film[b])	0.70/0.28	0.67/0.32
HOMO/LUMO [eV][c]	5.8/2.7	5.8/2.7
E_S [eV][d]/E_T [eV][e]	3.02/2.67	2.88/2.67
ΔE_{ST} [eV]	0.35	0.21

[a]Measured in CH_2Cl_2 solution (10^{-5} M); [b]Measured in film; [c]LUMO was measured from the onset of reduction potentials, HOMO was deduced from LUMO and E_g; [d]Singlet energy measured for the diluted solution at 298 K; [e]Triplet energy measured in 2-MeTHF at 77 K (10^{-5} M); [f]Not observed.

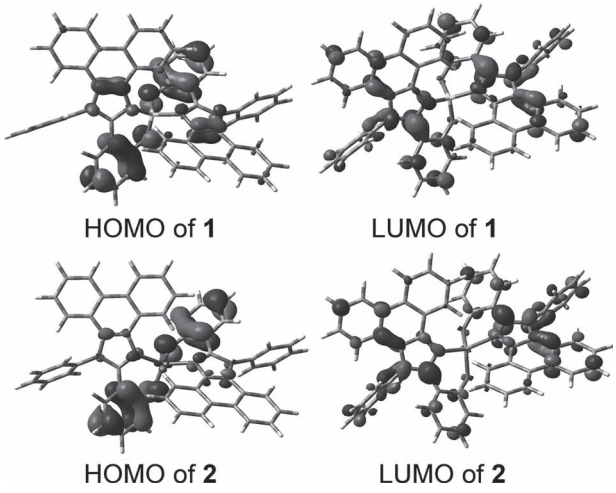

Figure 3. Calculated spatial distributions of the HOMO and LUMO levels of $Be(PPI)_2$ (**1**) and $Zn(PPI)_2$ (**2**).

2.4. Electrochemical Properties and Theoretical Calculations

The electrochemical behaviors were probed by cyclic voltammetry (CV). The LUMO energy levels were determined to be 2.7 eV from the onset of the reduction potentials with regard to ferrocene (see Supporting Information Figure S2).[13] Because no clear oxidation waves were observed, the HOMO energy levels were deduced to be 5.8 eV from LUMO energy levels and energy gaps determined by the onset of absorption. All data are summarized in Table 1. To gain insight into the structure–property relationship of the complexes at the molecular level, the geometrical and electronic structures of the complexes were studied using density functional theory (DFT). According to the DFT calculations of $Be(PPI)_2$, the two dihedral angles between the N−Be−O planes are 76°, which is close to the experimental values of 83° from the single-crystal X-ray diffraction (XRD) analysis. Such a highly twisting conformation may effectively suppress the more strong intermolecular interactions of their π systems and crystallinity, consequently leading to high PL efficiency and a stable amorphous thin film. The molecular orbital distribution of $Be(PPI)_2$ and $Zn(PPI)_2$ is shown in **Figure 3**. The HOMOs are mainly localized at the phenol group and imidazole ring, whereas the LUMOs are situated on the *N*-phenyl ring and phenanthroimidazole moiety, which explains the fact that their HOMO and LUMO energy level values are nearly the same. The adequate separation between the HOMO and LUMO benefits the efficient hole- and electron-transport properties (bipolar), prevents reverse energy transfer, and reduces the singlet–triplet splitting.

2.5. Single-Carrier Devices

To evaluate the carrier-transport character of the complexes, single-carrier devices of the host and doping films with the structures [ITO/MoO_3 (10 nm)/host (ITO = indium tin oxide) or host:dopant (60 nm)/MoO_3 (10 nm)/Al (100 nm)] for the hole-only device and [ITO/TPBI (10 nm)/host (TPBI = 1,3,5-tris (*N*-phenylbenzimidazol-2-yl)benzene) or host:dopant (60 nm)/LiF (1 nm)/Al (100 nm)] for the electron-only device were fabricated (see **Figure 4** and **Figure 5**).[14] For the hole-only devices, due to the large energy-injection barrier between the MoO_3 (LUMO = –2.3 eV) and Al (–4.3 eV) layers, only holes can be injected from the anode to the organic layer. In the electron-only devices, an additional thin TPBI layer, which has a low-lying HOMO level of –6.2 eV, was inserted as a hole-blocking layer to prevent the injection of holes from ITO (–4.8 eV) to the organic layer and ensure a pure electron current in the device. The *I–V* characteristics of single-carrier devices documented that $Be(PPI)_2$ and $Zn(PPI)_2$ are capable of transporting both electrons and holes (with significant currents and similar magnitudes to the complete OLED devices). Pure $Be(PPI)_2$ and $Be(PPI)_2$ doped with phosphorescent emitter possess a more balanced charge-transport ability than $Zn(PPI)_2$. A rational explanation for the ambipolar transport property of Be^{II} and Zn^{II} is that the phenol group and phenanthroimidazole moiety enable transport of the hole and electron, respectively. The phenol groups with electron-donating nature may enhance the hole-transporting ability of the resulting complexes. As we know, the carrier (including hole and electron) transporting properties of organic semiconductors are very sensitive to molecular structure, molecular

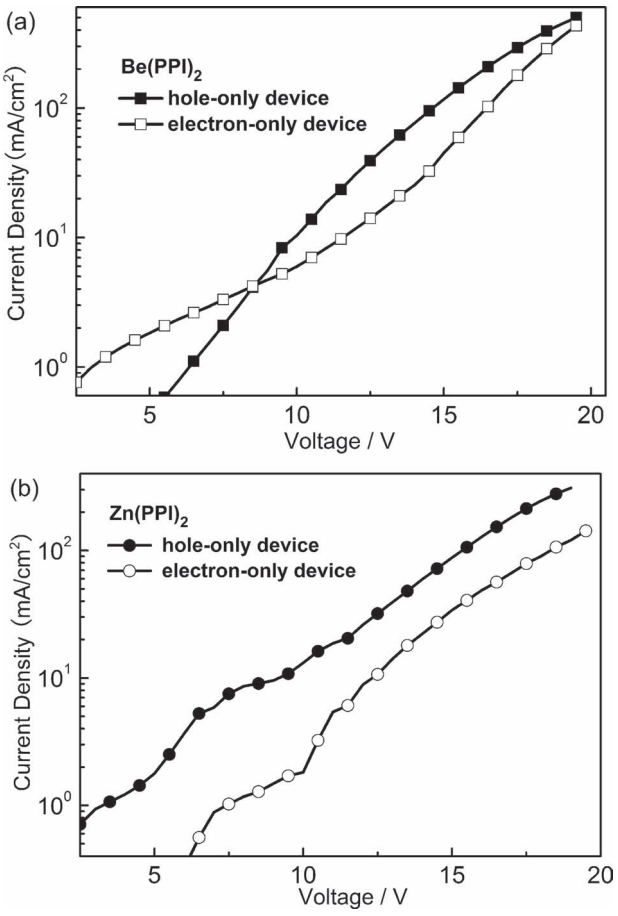

Figure 4. Current density versus voltage characteristics of the hole-only and electron-only devices for a) $Be(PPI)_2$ and b) $Zn(PPI)_2$.

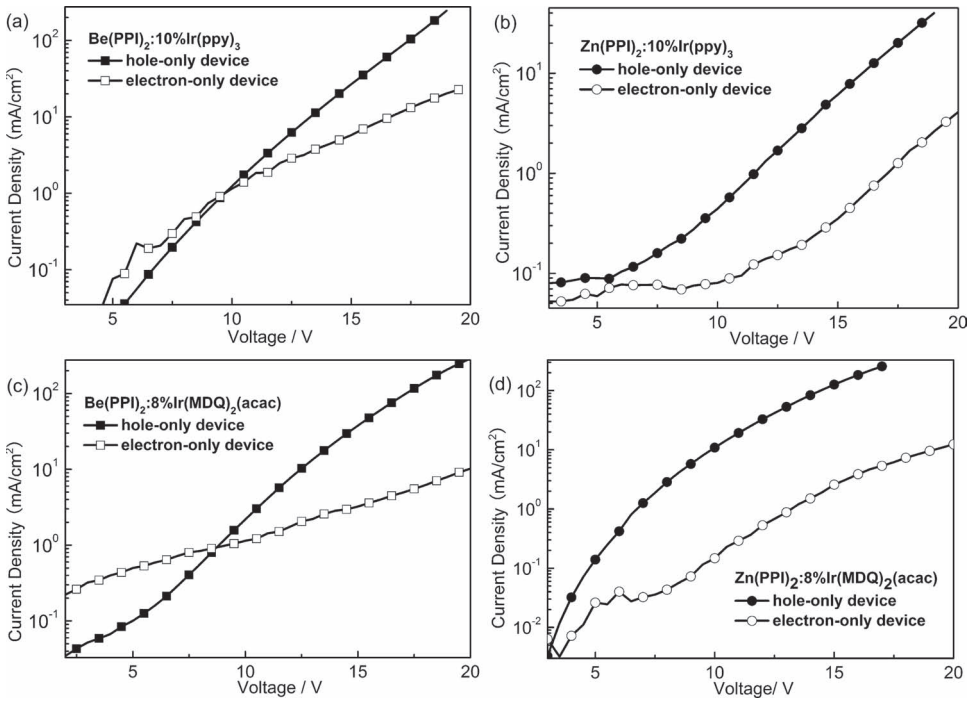

Figure 5. Current density versus voltage characteristics of the hole-only and electron-only devices for a) $Be(PPI)_2$ doped with 10 wt% $Ir(ppy)_3$, b) $Zn(PPI)_2$ doped with 10 wt% $Ir(ppy)_3$, c) $Be(PPI)_2$ doped with 8 wt% $Ir(MDQ)_2(acac)$, and d) $Zn(PPI)_2$ doped with 8 wt% $Ir(MDQ)_2(acac)$. $Ir(ppy)_3$ = *fac*-tris(2-phenylpyridine) iridium(III), $Ir(MDQ)_2(acac)$ = bis(2-methyldibenzo-[*f*,*h*]quinoxaline) acetylacetonate iridium(III).

configuration, as well as molecular packing modes in the solid state. Although $Be(PPI)_2$ and $Zn(PPI)_2$ have the same organic ligand, PPI, the central ions of Be^{II} and Zn^{II} possessing obviously different electronic structures and atom radius might have unequal impact on the chelated ligands, thus resulting in different semiconducting characteristics. On the other hand, intermolecular interactions in $Be(PPI)_2$ and $Zn(PPI)_2$ solids may be different, which also heavily influences the charge transporting nature. Following these considerations, the different single-carrier density between $Be(PPI)_2$ and $Zn(PPI)_2$ should be attributed to the different electronic structures of the central ions (Be^{2+} and Zn^{2+}), molecular structures, and packing in the solid state. The mobility of the molecules and the doped films was estimated from the single-carrier devices based on the space-charge-limited current (SCLC) method.[15] The calculated results indicate that both compounds have bipolar transport ability (**Table 2**). In addition, the mobilities of $Be(PPI)_2$ and $Be(PPI)_2$ doped with phosphorescent dye films are slightly higher and more balanced than that of $Zn(PPI)_2$-based films, which could support the following explanation on the lower roll-off of the devices based on $Be(PPI)_2$.

Table 2. SCLC hole and electron mobilities of hosts and host:dopant.

Compound	μ_h [$cm^2\ V^{-1}\ s^{-1}$]	μ_e [$cm^2\ V^{-1}\ s^{-1}$]
$Be(PPI)_2$	2.83×10^{-5}	7.47×10^{-5}
$Zn(PPI)_2$	3.97×10^{-5}	8.35×10^{-6}
$Be(PPI)_2$:10 wt% $Ir(ppy)_3$	4.32×10^{-6}	7.84×10^{-6}
$Zn(PPI)_2$:10 wt% $Ir(ppy)_3$	5.41×10^{-6}	1.02×10^{-6}
$Be(PPI)_2$:8 wt% $Ir(MDQ)_2(acac)$	6.87×10^{-6}	8.82×10^{-6}
$Zn(PPI)_2$:8 wt% $Ir(MDQ)_2(acac)$	6.46×10^{-6}	7.32×10^{-7}

2.6. Undoped Deep-Blue-Emitting OLEDs

We initially examined the performance of undoped deep-blue-emitting devices with the structure [ITO/MoO_3 (10 nm)/NPB (60 nm)/TCTA (5 nm)/$Be(PPI)_2$ or $Zn(PPI)_2$ (30 nm)/TPBI (30 nm)/LiF (1 nm)/Al (100 nm)] (device **B1** with emitting layer composed of $Be(PPI)_2$ and device **B2** with emitting layer composed of $Zn(PPI)_2$). In devices **B1** and **B2**, 1,4-bis[(1-naphthylphenyl)amino]-biphenyl (NPB) was used as the hole-transport material, and 4,4′,4″-tri(*N*-carbazolyl)triphenylamine (TCTA) was used as the electron-blocking layer as well as triplet exciton blocker layer in the PhOLEDs. 1,3,5-Tris(*N*-phenylbenzimidazol-2-yl)benzene (TPBI) was utilized as the electron-transport and hole-blocking material, and MoO_3 and LiF served as hole- and electron-injecting layer, respectively. Both devices **B1** and **B2** exhibit deep-blue emissions with Commission International de l'Eclairage (CIE) coordinates of (0.15, 0.09), which is very close to the NTSC (National Television Standards Committee) blue standard (CIE: 0.14, 0.08) and remains almost unchanged over a wide range of driving voltage. Device **B1** using $Be(PPI)_2$ as emitter exhibited a turn-on voltage of 3.2 V. The maximum external quantum ($\eta_{ext.max}$), current ($\eta_{c.max}$), and power ($\eta_{p.max}$) efficiencies of this device are 2.82%, 2.41 cd A^{-1}, and 2.52 lm W^{-1}, respectively. Device **B2** using $Zn(PPI)_2$ as emitter

Table 3. Electroluminescence properties of the devices.[a)]

	Dopant	V_{on} [V]	L_{max} [cd m^{-2}]	η_c[b)] [cd A^{-1}]	η_p[b)] [lm W^{-1}]	η_{ext}[b)] [%]	CIE(x,y)[c)]
B1	–	3.2	2745	2.41, 2.18, 2.04	2.52, 1.60, 0.95	2.82, 2.55, 2.40	0.15,0.09
B2	–	3.2	1669	2.06, 1.31, 0.74	2.02, 0.75, 0.26	2.08, 1.32, 0.75	0.15,0.09
G1	Ir(ppy)$_3$	2.7	92 261	55.6, 54.9, 53.5	61.4, 48.8, 36.1	15.3, 15.2, 14.7	0.32,0.61
G2	Ir(ppy)$_3$	2.7	85 872	58.0, 53.2, 50.7	67.5, 49.1, 35.8	15.9, 14.6, 13.9	0.30,0.63
R1	Ir(MDQ)$_2$(acac)	2.3	38 580	15.9, 15.4, 13.9	19.9, 17.5, 12.6	15.1, 14.7, 13.3	0.64,0.36
R2	Ir(MDQ)$_2$(acac)	2.3	39 138	15.9, 11.3, 10.7	21.7, 8.48, 4.83	15.2, 10.8, 10.2	0.64,0.36

[a)]Abbreviations: V_{on} = turn-on voltage, L_{max} = maximum luminance, η_c = maximum current efficiency, η_p = maximum power efficiency, η_{ext} = maximum external quantum efficiency; [b)]In the order of maximum, then values at 100 and 1000 cd m^{-2}; [c)]Measured at 100 cd m^{-2}.

showed a slightly lower performance than device **B1** (**Table 3**). It is worth noting that the external quantum efficiency roll-off for device **B1** is smaller than that of device **B2**, which indicates a well-balanced charge-transport property in device **B1**. The power efficiency (lm W^{-1}) of device **B1** is comparable with the highest value reported for undoped deep-blue OLEDs with CIE $y < 0.10$.[4]

2.7. Phosphorescent OLEDs

To investigate the utility of these two complexes as host materials for green and red phosphorescent emitters, we fabricated devices with the following configurations: [ITO/MoO_3 (10 nm)/NPB (60 nm)/TCTA (5 nm)/Be(PPI)$_2$ or Zn(PPI)$_2$:Ir(ppy)$_3$ (30 nm)/TPBI (30 nm)/LiF (1 nm)/Al (100 nm)] (devices **G1** and **G2**) and [ITO/MoO_3 (10 nm)/NPB (60 nm)/TCTA (5 nm)/Be(PPI)$_2$ or Zn(PPI)$_2$:Ir(MDQ)$_2$(acac) (30 nm)/TPBI (30 nm)/LiF (1 nm)/Al (100 nm)] (devices **R1** and **R2**). In these devices, green-emissive *fac*-tris(2-phenylpyridine) iridium(III) (Ir(ppy)$_3$) or red-emissive bis(2-methyldibenzo-[*f*,*h*]quinoxaline) acetylacetonate iridium(III) (Ir(MDQ)$_2$(acac)) was doped in Be(PPI)$_2$ or Zn(PPI)$_2$ to form the emitting layer with an optimized doping concentration of 10 wt% for Ir(ppy)$_3$ and 8 wt% for Ir(MDQ)$_2$(acac). **Figure 6** presents the energy level diagram of the materials used and the molecular structures of the phosphorescent dyes Ir(ppy)$_3$ and Ir(MDQ)$_2$(acac).

The current density–voltage–brightness (*J*–*V*–*L*) characteristics, current efficiencies, and power efficiencies versus current density curves of devices **B1**, **B2**, **G1**, **G2**, **R1**, and **R2** are shown in **Figure 7** and Figure S3, respectively. Remarkably, device **G1** showed rather lower efficiency roll-off than device **G2** at high brightness. For instance, device **G1** exhibited η_c of 53.5 cd A^{-1} and η_{ext} of 14.7% with an external quantum efficiency roll-off of 3.3% at the luminance of 1000 cd m^{-2}, while the corresponding performance values for device **G2** are 50.7 cd A^{-1}, 13.9%, and roll-off of 12.5%. Even when the brightness reached as high as 10 000 cd m^{-2}, η_c was still maintained at 46.1 cd A^{-1} (η_{ext} = 12.8%) with efficiency roll-off of 12% for device **G1**. Furthermore, good performance of red electrophosphorescence was also achieved by devices **R1** and **R2**. The bipolar property and suitable energy levels of Be(PPI)$_2$ and Zn(PPI)$_2$ promote facile charge injections from the carrier-transport layers to the emitter layer, which results in a low turn-on voltage of 2.3 V. The

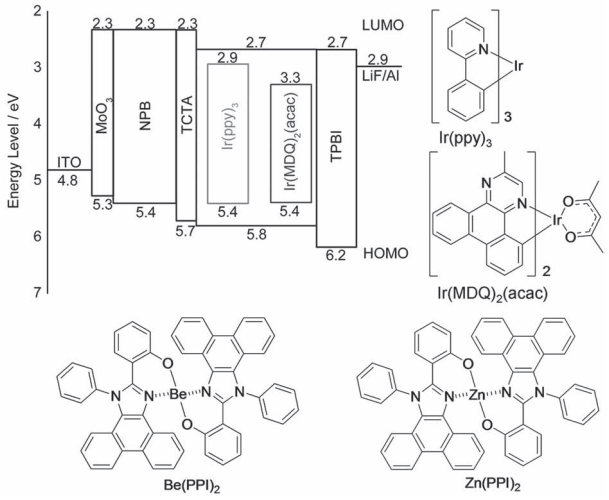

Figure 6. Energy level diagram of the materials used and the chemical structures of the fluorescent and phosphorescent materials.

maximum luminance (L_{max}), current efficiency ($\eta_{c.max}$), power efficiency ($\eta_{p.max}$), and external quantum efficiency ($\eta_{ext.max}$) are 38 580 cd m^{-2}, 15.9 cd A^{-1}, 19.9 lm W^{-1}, and 15.1%, respectively, for device **R1** and 39 138 cd m^{-2}, 15.9 cd A^{-1}, 21.7 lm W^{-1}, and 15.2%, respectively, for device **R2**. These values are comparable to those of recently reported highly efficient saturated red PhOLEDs.[2] The electroluminescence spectra of **R1** and **R2** did not exhibit any other residual emission and showed approximately saturated red emissions with CIE (**0.64**, 0.36). This observation reflects a complete energy transfer from hosts to dopant. In addition, the current density and brightness of device **R1** rise more rapidly than those for device **R2**, which should be attributed to the fact that Be(PPI)$_2$ possesses a higher and more balanced carrier-transport property than Zn(PPI)$_2$, as revealed by the characteristics of their single-carrier devices. Similar to the performance of the green devices, device **R1** also exhibits a significantly lower-efficiency roll-off than **R2**. The current efficiencies of **R1** at 100 and 1000 cd m^{-2} are still as high as 15.4 cd A^{-1} (η_{ext} = 14.7%) and 13.9 cd A^{-1} (η_{ext} = 13.3%), with roll-off of 2.6 and 11.9%, respectively. A possible explanation for the low-efficiency roll-off behavior of the Be(PPI)$_2$-based device is

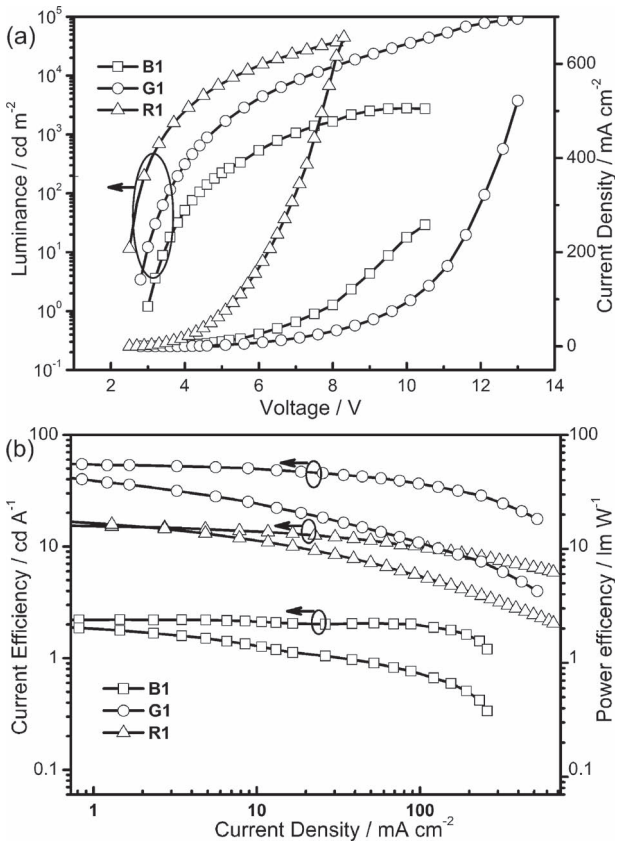

Figure 7. a) Current density–voltage–brightness (*J–V–L*) characteristics. b) Current efficiency and power efficiency versus current density curves for devices **B1**, **G1**, and **R1** based on $Be(PPI)_2$.

that the more balanced carrier transport (Figure 5) may lead to a broader distribution of the recombination region within the emission layer. Both the hole and electron can be efficiently injected and well-distributively dispersed in the bipolar emitting layer. Therefore, within the whole emitting layer the recombination between hole and electron may take place resulting in an exciton generation zone including the whole emitting layer. The excited phosphors dispersed in a wider region may efficiently reduce the probability of a triplet–triplet annihilation (TTA) process, which usually causes phosphorescence quenching at high current density.

The electroluminescence spectra and CIE coordinates of devices **B1**, **G1**, and **R1** are shown in **Figure 8** and those of devices **B2**, **G2**, and **R2** are displayed in Figure S4 (see Supporting Information). The device performance data for **B1**, **B2**, **G1**, **G2**, **R1**, and **R2** is summarized in Table 3. Clearly, R, G, and B electroluminescence spectra with very high color purity have been achieved by using a simple material system. To the best of our knowledge, $Be(PPI)_2$ and $Zn(PPI)_2$ are the first kind of ambipolar coordination complex that can be employed as host material to fabricate high-performance green and red PhOLEDs. We have not yet studied the lifetime of the devices, but the unencapsulated devices were electrically stable, and the emission color and the *I –L–V* did not change during the measurement of electroluminescence data in air.

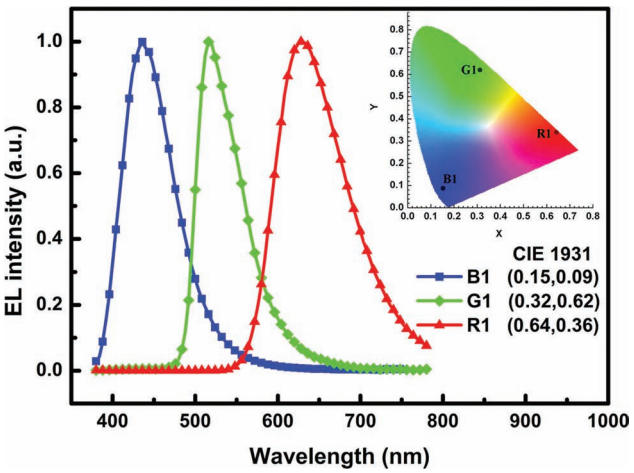

Figure 8. Electroluminescence (EL) spectra and CIE1931 coordinates of devices **B1**, **G1**, and **R1** based on $Be(PPI)_2$.

3. Conclusion

In summary, two luminescent coordination complexes, $Be(PPI)_2$ and $Zn(PPI)_2$, with ambipolar transport nature as well as small singlet–triplet splitting feature have been designed and synthesized. The complexes have not only been used as emitters to fabricate deep-blue OLEDs, but also as host materials to construct highly efficient green and red PhOLEDs. The small singlet–triplet splitting ensures that the singlet energy of $Be(PPI)_2$ and $Zn(PPI)_2$ can offer true blue emission, and the triplet energy is sufficient to excite the green and red phosphors. The relatively balanced carrier-transport property allowed the phosphor-doped $Be(PPI)_2$ and $Zn(PPI)_2$ films to show relatively high electroluminescence power efficiency. Particularly, the $Be(PPI)_2$-based devices exhibited lower-efficiency roll-off than $Zn(PPI)_2$-based ones, which could be attributed to the more balanced carrier-transport characteristic of $Be(PPI)_2$. Our study presents a new strategy for the molecular design of multifunctional materials with efficient bipolar transport and deep-blue emitting properties.

4. Experimental Section

General Information: ^1H NMR spectra were measured on a Varian Mercury 300 MHz spectrometer with tetramethylsilane as the internal standard. Mass spectra were recorded on a Shimadzu AXIMA-CFR MALDI-TOF mass spectrometer. Elemental analyses were performed on a flash EA 1112 spectrometer. UV-vis absorption spectra were recorded by a Shimadzu UV-2550 spectrophotometer. The emission spectra were recorded by a Shimadzu RF-5301 PC spectrometer. The absolute fluorescence quantum yields of solutions and films were measured on an Edinburgh FLS920 steady-state fluorimeter (excited at 365 nm). Differential scanning calorimetry (DSC) measurements were performed on a NETZSCH DSC204 instrument at a heating rate of 10 °C min^{-1} from 20 to 420 °C under a nitrogen atmosphere. Thermogravimetric analysis (TGA) was performed on a TA Q500 thermogravimeter by measuring the weight loss while heating at a rate of 10 °C min^{-1} from 25 to 800 °C under nitrogen. Electrochemical measurements were performed with a BAS 100 W Bioanalytical electrochemical workstation, using Pt as working electrode, platinum wire as auxiliary electrode, and a porous

glass wick Ag/Ag^+ as pseudo-reference electrode standardized against ferrocene/ferrocenium. The reduction potentials were measured in DMF solution containing 0.1 M *n*-Bu_4NPF_6 as supporting electrolyte at a scan rate of 100 mV s^{-1}.

Single-Crystal Structure: A single crystal suitable for X-ray structural analysis was obtained by vacuum sublimation. Diffraction data were collected on a Rigaku RAXIS-PRID diffractometer using the ω-scan mode with graphite-monochromator MoKα radiation. The structure was solved with direct methods using the SHELXTL programs and refined with full-matrix least squares on F^2.[16] Non-hydrogen atoms were refined anisotropically. The positions of hydrogen atoms were calculated and refined isotropically. The corresponding CCDC reference number (CCDC: 888112) and the data can be obtained free of charge from The Cambridge Crystallographic Data Centre via www.ccdc.cam.ac.uk/data_request/cif.

Preparation of Materials: Tetrabutylammonium hexafluorophosphate (Bu_4NPF_6) was purchased from Aldrich. 1,3,5-Tris-(*N*-phenylbenzimidizol-2-yl)benzene (TPBI), 1,4-bis[(1-naphthylphenyl)amino]-biphenyl (NPB), and 4,4′,4″-tri(*N*-carbazolyl)triphenylamine (TCTA) were prepared and purified by sublimation prior to use. All commercially available reagents were used as received unless otherwise stated. All reactions were carried out using Schlenk techniques under a nitrogen atmosphere.

Synthesis of 2-(1-phenyl-1H-phenanthro[9,10-d]imidazol-2-yl)phenol (PPIH): A mixture of phenanthrenequinone (2.08 g, 10 mmol), 2-hydroxybenzaldehyde (1.46 g, 12 mmol), aniline (4.46 g, 48 mmol), ammonium acetate (2.96 g, 38.4 mmol), and glacial acetic acid (60 mL) was heated at 100 °C for 3 h under a nitrogen atmosphere. After cooling to room temperature, the reaction mixture was poured into distilled water with stirring. The separated solid was isolated by filtration, washed with water, and dried to give a pale solid. The solid was then purified by column chromatography on silica gel using CH_2Cl_2/petroleum (1:1 v/v) as the eluent to give the product. Yield: 56%; ^{1}H NMR (300 MHz, $CDCl_3$): δ = 11.83 (s, 1H; OH), 8.95 (d, *J* = 8.4 Hz, 1H; Ar H), 8.90 (d, *J* = 8.4 Hz, 1H; Ar H), 8.61 (d, *J* = 7.8 Hz, 1H; Ar H), 7.81 (t, *J* = 7.2 Hz, 1H; Ar H), 7.76–7.64 (m, 6H; Ar H), 7.57 (t, *J* = 7.8 Hz, 1H; Ar H), 7.34 (t, *J* = 7.8 Hz, 1H; Ar H), 7.26 (t, *J* = 7.8 Hz, 1H; Ar H), 7.03 (t, *J* = 7.2 Hz, 2H; Ar H), 6.94 (d, *J* = 8.1 Hz, 1H; Ar H), 6.66 ppm (d, *J* = 7.5 Hz, 1H; Ar H); MALDI-TOF MS (M): *m*/*z*: calcd: 386.1 [*M*+H]$^+$; found: 385.8; elemental analysis calcd (%) for $C_{27}H_{18}N_2O$: C 83.92, H 4.69, N 7.25; found: C 83.85, H 4.42, N 7.11.

Synthesis of Be(PPI)$_2$: $BeSO_4{\cdot}5H_2O$ (0.265 g, 1.5 mmol) dissolved in distilled water (1 mL) was slowly added to a 100 mL round-bottomed flask containing PPIH (1.158 g, 3 mmol) and methanol (50 mL). The pH of the solution was adjusted to 10 with sodium hydroxide and the solution was refluxed for 12 h, during which a pale yellow solid precipitated from the solution. After cooling to room temperature, the residue was collected by filtration and the crude product was purified by the train sublimation method to give $Be(PPI)_2$. Yield: 40%; ^{1}H NMR (300 MHz, [D_6]DMSO): δ = 8.83 (d, *J* = 8.4 Hz, 1H; Ar H), 8.08 (d, *J* = 7.8 Hz, 1H; Ar H), 7.98 (d, *J* = 8.4 Hz, 1H; Ar H), 7.85–7.72 (m, 5H; Ar H), 7.52 (t, *J* = 7.8 Hz, 1H; Ar H), 7.32–7.13 (m, 2H; Ar H), 7.13 (t, *J* = 7.8 Hz, 1H; Ar H), 6.93 (t, *J* = 8.1 Hz, 1H; Ar H), 6.86 (d, *J* = 7.8 Hz, 1H; Ar H), 6.78 (t, *J* = 9 Hz, 2H; Ar H), 6.27 ppm (t, *J* = 7.5 Hz, 1H; Ar H); MALDI-TOF MS (M): *m*/*z*: calcd: 779.3 [*M*+H]$^+$; found: 778.7; elemental analysis calcd (%) for $C_{54}H_{34}BeN_4O_2$: C 83.16, H 4.39, N 7.18; found: C 82.87, H 4.25, N 6.96.

Synthesis of Zn(PPI)$_2$: $Zn(PPI)_2$ was synthesized by a procedure similar to that for $Be(PPI)_2$ except that $Zn(OAc)_2{\cdot}2H_2O$ was used as the reactant instead of $BeSO_4{\cdot}5H_2O$. Yield: 48%; ^{1}H NMR (300 MHz, [D_6]DMSO): δ = 8.83 (d, *J* = 8.4 Hz, 1H; Ar H), 8.08 (d, *J* = 7.8 Hz, 1H; Ar H), 7.98 (d, *J* = 8.4 Hz, 1H; Ar H), 7.85–7.72 (m, 5H; Ar H), 7.52 (t, *J* = 7.8 Hz, 1H; Ar H), 7.32–7.13 (m, 2H; Ar H), 7.13 (t, *J* = 7.8 Hz, 1H; Ar H), 6.93 (t, *J* = 8.1 Hz, 1H; Ar H), 6.86 (d, *J* = 7.8 Hz, 1H; Ar H), 6.78 (t, *J* = 9 Hz, 2H; Ar H), 6.27 ppm (t, *J* = 7.5 Hz, 1H; Ar H); MALDI-TOF MS (M): *m*/*z*: calcd: 833.5 [*M*+H]$^+$; found: 834.2; elemental analysis calcd for $C_{54}H_{34}ZnN_4O_2$: C 77.56, H 4.10, N 6.70; found: C 77.41, H 4.04, N 6.56.

Theoretical Calculations: The ground-state geometries were fully optimized by the density functional theory (DFT)[17] method with the Becke three-parameter hybrid exchange and the Lee–Yang–Parr correlation functional[18] (B3LYP) and 6-31G* basis set using the Gaussian 03 software package.[19]

Device Fabrication and Measurement: Before device fabrication, the ITO glass substrates were precleaned carefully and treated by UV/O_3 for 2 min. Then the sample was transferred to the deposition system. The devices were prepared in vacuum at a pressure of 5×10^{-6} Torr. The hole-injection material MoO_3, hole-transporting material NPB, exciton blocking material TCTA, and hole-blocking and electron-transporting material TPBI were thermally evaporated at a rate of 1.0 Å s^{-1}. After the organic film deposition, 1 nm of LiF and 100 nm of aluminum were thermally evaporated onto the organic surface. The thicknesses of the organic materials and the cathode layers were controlled by using a quartz crystal thickness monitor. All of the organic materials used were purified by a vacuum sublimation approach. The electrical characteristics of the devices were measured with a Keithley 2400 source meter. The electroluminescence spectra and luminance of the devices were obtained on a PR650 spectrometer. All the device fabrication and characterization steps were carried out at room temperature under ambient laboratory conditions. Current–voltage characteristics of single-carrier devices were measured using the same semiconductor parameter analyzer as for PhOLED devices. The single-carrier device measurements were performed under dark and ambient conditions.

Supporting Information

Supporting Information is available from the Wiley Online Library or from the author.

Acknowledgements

This work was supported by the National Natural Science Foundation of China (51173065 and 20921003) and National Basic Research Program of China (973 Program, 2009CB623600).

Received: October 13, 2012
Revised: November 15, 2012
Published online: December 21, 2012

[1] a) M. A. Baldo, M. E. Thompson, S. R. Forrest, *Nature* **2000**, *403*, 750; b) S. Reineke, F. Lindner, G. Schwartz, N. Seidler, K. Walzer, B. Lüssem, K. Leo, *Nature* **2009**, *459*, 234; c) A. C. Grimsdale, K. L. Chan, R. E. Martin, P. G. Jokisz, A. B. Holmes, *Chem. Rev.* **2009**, *109*, 897.

[2] a) Y. L. Tung, S. W. Lee, Y. Chi, Y. T. Tao, C. H. Chien, Y. M. Cheng, P. T. Chou, S. M. Peng, C. S. Liu, *J. Mater. Chem.* **2005**, *15*, 460; b) Y. Tao, Q. Wang, C. Yang, Q. Wang, Z. Zhang, T. Zou, J. Qin, D. Ma, *Angew. Chem. Int. Ed.* **2008**, *120*, 8224; c) Y. Y. Lyu, J. Kwak, W. S. Jeon, Y. Byun, H. S. Lee, D. Kim, C. Lee, K. Char, *Adv. Funct. Mater.* **2009**, *19*, 420; d) J. Kwak, Y. Lyu, H. Lee, B. Choi, K. Char, C. Lee, *J. Mater. Chem.* **2012**, *22*, 6351; e) J. Duan, P. Sun, C. Cheng, *Adv. Mater.* **2003**, *15*, 224; f) C. H. Fan, P. P. Sun, T. H. Su, C. H. Cheng, *Adv. Mater.* **2011**, *23*, 2981; g) D. H. Kim, N. S. Cho, H. Y. Oh, J. H. Yang, W. S. Jeon, J. S. Park, M. C. Suh, J. H. Kwon, *Adv. Mater.* **2011**, *23*, 2721; h) H. H. Chou, C. H. Cheng, *Adv. Mater.* **2010**, *22*, 2468; i) H. Fukagawa, T. Shimizu, H. Hanashima, Y. Osada, M. Suzuki, H. Fujikake, *Adv. Mater.* **2012**, *24*, 5099; j) Y. Cho, J. Lee, *Adv. Mater.* **2011**, *23*, 4568.

[3] a) H.-F. Chen, S.-J. Yang, Z.-H. Tsai, W.-Y. Hung, T.-C. Wang, K.-T. Wong, *J. Mater. Chem* **2012**, *22*, 6351; b) Y. Zhu, L. Zhou, H. Li, Q. Xu, M. Teng, Y. Zheng, J. Zuo, H. Zhang, X. You, *Adv. Mater.* **2011**, *23*, 4041; c) C.-H. Chang, M.-C. Kuo, W.-C. Lin, Y.-T. Chen, K.-T. Wong, S.-H. Chou, E. Mondal, R. C. Kwong,

S. Xia, T. Nakagawa, C. Adachi, *J. Mater. Chem* **2012**, *22*, 3832; d) M. Hashimoto, S. Igawa, M. Yashima, I. Kawata, M. Hoshino, M. Osawa, *J. Am. Chem. Soc.* **2011**, *133*, 10348; e) S. Gong, Y. Zhao, C. Yang, C. Zhong, J. Qin, D. Ma, *J. Phys. Chem. C* **2010**, *114*, 5193; f) Y. Tao, Q. Wang, C. Yang, C. Zhong, K. Zhang, J. Qin, D. Ma, *Adv. Funct. Mater.* **2009**, *20*, 304.

[4] a) Y. Wei, C. T. Chen, *J. Am. Chem. Soc.* **2007**, *129*, 7478; b) C. Chein, C. Chen, F. Hsu, C. Shu, P. Chou, C. Lai, *Adv. Funct. Mater.* **2009**, *19*, 560; c) Z. Jiang, Z. Liu, C. Yang, C. Zhong, J. Qin, G. Yu, Y. Liu, *Adv. Funct. Mater.* **2010**, *12*, 452; d) C. Zheng, W. Zhao, Z. Wang, D. Huang, J. Ye, X. Qu, X. Zhang, C. Lee, S. Lee, *J. Mater. Chem.* **2010**, *20*, 1560; e) J. Seo, K. Lee, B. Seo, J. Koo, S. Moon, J. Park, S. Yoon, Y. Kim, *Org. Electron.* **2010**, *11*, 905; f) Y. Zhang, S. L. Lai, Q. X. Tong, M. F. Lo, T. W. Ng, M. Y. Chan, Z. C. Wen, J. He, K. S. Jeff, X. L. Tang, W. M. Liu, C. C. Ko, P. F. Wang, C. S. Lee, *Chem. Mater.* **2012**, *24*, 61; g) S. Gong, Y. Zhao, M. Wang, C. Yang, C. Zhong, J. Qin, D. Ma, *Chem. Asian J.* **2010**, *5*, 2093; h) S. K. Kim, B. Yang, Y. Ma, J. H. Leec, J. Park, *J. Mater. Chem.* **2008**, *18*, 3376; i) D. Thirion, M. Romain, J. Rault-Berthelot, C. Poriel, *J. Mater. Chem.* **2012**, *22*, 7149; j) C. Poriel, N. Cocherel, J. Rault-Berthelot, L. Vignau, O. Jeannin, *Chem. Eur. J.* **2011**, *17*, 12631; k) A. L. Fischer, K. E. Linton, K. T. Kamtekar, C. Pearson, M. R. Bryce, M. C. Petty, *Chem. Mater.* **2011**, *23*, 1640; l) K. E. Linton, A. L. Fischer, C. Pearson, M. A. Fox, L.-O. Palsson, M. R. Bryce, M. C. Petty, *J. Mater. Chem.* **2012**, *22*, 11816; m) X. Xing, L. Xiao, L. Zheng, S. Hu, Z. Chen, B. Qu, Q. Gong, *J. Mater. Chem.* **2012**, *22*, 15136; n) M. Zhu, Q. Wang, Y. Gu, X. Cao, C. Zhong, D. Ma, J. Qin, C. Yang, *J. Mater. Chem.* **2011**, *21*, 6409.

[5] a) S. Chen, G. Tan, W.-Y. Wong, H.-S. Kwok, *Adv. Funct. Mater.* **2011**, *21*, 3785; b) G. M. Farinola, R. Ragni, *Chem. Soc. Rev.* **2011**, *40*, 3467; c) S. L. Gong, Y. H. Chen, J. J. Luo, C. L. Yang, C. Zhong, J. G. Qin, D. G. Ma, *Adv. Funct. Mater.* **2011**, *21*, 1168; d) B. P. Yan, C. C. C. Cheung, S. C. F. Kui, H. F. Xiang, V. A. L. Roy, S. J. Xu, C. M. Che, *Adv. Mater.* **2007**, *19*, 3599; e) H. Sasabe, J. I. Takamatsu, T. Motoyama, S. Watanabe, G. Wagenblast, N. Langer, O. Molt, E. Fuchs, C. Lennartz, J. Kido, *Adv. Mater.* **2010**, *22*, 5003; f) R. J. Wang, D. Liu, H. C. Ren, T. Zhang, H. M. Yin, G. Y. Liu, J. Y. Li, *Adv. Mater.* **2011**, *23*, 2823; g) K. T. Kamtekar, A. P. Monkman, M. R. Bryce, *Adv. Mater.* **2010**, *22*, 572; h) M. C. Gather, A. Köhnen, K. Meerholz, *Adv. Mater.* **2011**, *23*, 233.

[6] a) H. Sasabe, N. Toyota, H. Nakanishi, T. Ishizaka, Y. J. Pu, J. Kido, *Adv. Mater.* **2012**, *24*, 3212; b) H. H. Chou, C. H. Cheng, *Adv. Mater.* **2010**, *22*, 2468; c) J. K. Bin, N. S. Cho, J. I. Hong, *Adv. Mater.* **2012**, *24*, 2911; d) H. Fukagawa, N. Yokoyama, S. Irisa, S. Tokito, *Adv. Mater.* **2010**, *22*, 4775; e) Z. Q. Gao, M. M. Luo, X. H. Sun, H. L. Tam, M. S. Wong, B. X. Mi, P. F. Xia, K. W. Cheah, C. H. Chen, *Adv. Mater.* **2009**, *21*, 688; f) S. Y. Shao, J. Q. Ding, T. L. Ye, Z. Y. Xie, L. X. Wang, X. B. Jing, F. S. Wang, *Adv. Mater.* **2011**, *23*, 3570; g) K. S. Yook, J. Y. Lee, *Adv. Mater.* **2012**, *24*, 3169; h) Z. Jiang, T. Ye, C. Yang, D. Yang, M. Zhu, C. Zhong, J. Qin, D. Ma, *Chem. Mater.* **2011**, *23*, 771; i) H. Sasabe, J. Kido, *Chem. Mater.* **2011**, *23*, 621.

[7] a) G. Schwartz, S. Reineke, T. C. Rosenow, K. Walzer, K. Leo, *Adv. Funct. Mater.* **2009**, *19*, 1319; b) G. Schwartz, M. Pfeiffer, S. Reineke, K. Walzer, K. Leo, *Adv. Mater.* **2007**, *19*, 3672.

[8] a) M. Y. Lai, C. H. Chen, W. S. Huang, J. T. Lin, T. H. Ke, L. Y. Chen, M. H. Tsai, C. C. Wu, *Angew. Chem. Int. Ed.* **2008**, *120*, 581; b) T. Peng, Y. Yang, H. Bi, Y. Liu, Z. Hou, Y. Wang, *J. Mater. Chem.* **2011**, *21*, 3551; c) J. Ye, C. J. Zheng, X. M. Qu, X. H. Zhang, M. K. Fung, C. S. Lee, *Adv. Mater.* **2012**, *24*, 3410.

[9] a) S. L. Gong, Q. Fu, Q. Wang, C. L. Yang, C. Zhong, J. G. Qin, D. G. Ma, *Adv. Mater.* **2011**, *23*, 4956; b) D. H. Yu, F. C. Zhao, C. M. Han, H. Xu, J. Li, Z. Zhang, Z. P. Deng, D. G. Ma, P. G. Yan, *Adv. Mater.* **2012**, *24*, 509; c) X. F. Ren, J. Li, R. J. Holmes, P. I. Djurovich, S. R. Forrest, M. E. Thompsom, *Chem. Mater.* **2004**, *16*, 4743; d) C. Han, Z. Zhang, H. Xu, J. Li, G. Xie, R. Chen, Y. Zhao, W. Huang, *Angew. Chem. Int. Ed.* **2012**, *51*, 10104; e) C. Poriel, R. Métivier, J. Rault-Berthelot, D. Thirion, F. Barrière, O. Jeannin, *Chem. Commun.* **2011**, *47*, 11703; f) J. Zhao, G. Xie, C. Yin, L. Xie, C. Han, R. Chen, H. Xu, M. Yi, Z. Deng, S. Chen, Y. Zhao, S. Liu, W. Huang, *Chem. Mater.* **2011**, *23*, 5331; g) G. Méhes, H. Nomura, Q. Zhang, T. Nakagawa, C. Adachi, *Angew. Chem. Int. Ed.* **2012**, *51*, 11311; h) Q. Zhang, J. Li, K. Shizu, S. Huang, S. Hirata, H. Miyazaki, C. Adachi, *J. Am. Chem. Soc.* **2012**, *134*, 14706.

[10] Y. Yuan, D. Li, X. Zhang, X. Zhao, Y. Liu, J. Zhang, Y. Wang, *New J. Chem.* **2011**, *35*, 1534.

[11] a) Y. Li, Y. Liu, W. Bu, D. Lu, Y. Wu, Y. Wang, *Chem. Mater.* **2000**, *12*, 2672; b) Y. Wang, W. Zhang, Y. Li, L. Ye, G. Yang, *Chem. Mater.* **1999**, *11*, 530.

[12] a) Y. N. Yan, W. L. Pan, H. C. Song, *Dyes Pigm.* **2010**, *86*, 249; b) M.-S. Tsai, Y.-C. Hsu, J.-T. Lin, H.-C. Chen, C.-P. Hsu, *J. Phys. Chem. C* **2007**, *111*, 18785.

[13] C. M. Cardona, W. Li, A. E. Kaifer, D. Stockdale, G. C. Bazan, *Adv. Mater.* **2011**, *23*, 2367.

[14] a) C. J. Zheng, J. Ye, M. F. Lo, M. K. Fung, X. M. Ou, X. H. Zhang, C. S. Lee, *Chem. Mater.* **2012**, *24*, 643; b) W. Jiang, L. Duan, J. Qiao, G. Dong, L. Wang, Y. Qiu, *Org. Lett.* **2011**, *13*, 3146; c) F. M. Hsu, C. H. Chien, Y. J. Hsieh, C. H. Wu, C. F. Shu, S. W. Liu, C. T. Chen, *J. Mater. Chem.* **2009**, *19*, 8002; d) S. J. Su, E. Gonmori, H. Sasabe, J. Kido, *Adv. Mater.* **2008**, *20*, 4189.

[15] a) P. W. M. Blom, M. J. M. De Jong, M. G. van Munster, *Phys. Rev. B* **1997**, *55*, 656; b) Y. H. Zhou, J. N. Pei, Q. F. Dong, X. B. Sun, Y. Q. Liu, W. J. Tian, *J. Phys. Chem. C* **2009**, *113*, 7882.

[16] SHELXTL, Version 5.1; Siemens Industrial Automation, Inc., **1997**; *G. M. Sheldrick, SHELXS-97, Program for Crystal Structure Solution*, University of Göttingen, Göttingen **1997**.

[17] E. Runge, E. K. U. Gross, *Phys. Rev. Lett.* **1984**, *52*, 997.

[18] A. D. J. Becke, *Chem. Phys.* **1993**, *98*, 5648.

[19] M. J. Frisch, G. W. Trucks, H. B. Schlegel, G. E. Scuseria, M. A. Robb, J. R. Cheeseman, J. A. Montgomery Jr., T. Vreven, K. N. Kudin, J. C. Burant, J. M. Millam, S. S. Iyengar, J. Tomasi, V. Barone, B. Mennucci, M. Cossi, G. Scalmani, N. Rega, G. A. Petersson, H. Nakatsuji, M. Hada, M. Ehara, K. Toyota, R. Fukuda, J. Hasegawa, M. Ishida, T. Nakajima, Y. Honda, O. Kitao, H. Nakai, M. Klene, X. Li, J. E. Knox, H. P. Hratchian, J. B. Cross, C. Adamo, J. Jaramillo, R. Gomperts, R. E. Stratmann, O. Yazyev, A. J. Austin, R. Cammi, C. Pomelli, J. W. Ochterski, P. Y. Ayala, K. Morokuma, G. A. Voth, P. Salvador, J. J. Dannenberg, V. G. Zakrzewski, S. Dapprich, A. D. Daniels, M. C. Strain, O. Farkas, D. K. Malick, A. D. Rabuck, K. Raghavachari, J. B. Foresman, J. V. Ortiz, Q. Cui, A. G. Baboul, S. Clifford, J. Cioslowski, B. B. Stefanov, G. Liu, A. Liashenko, P. Piskorz, I. Komaromi, R. L. Martin, D. J. Fox, T. Keith, M. A. Al-Laham, C. Y. Peng, A. Nanayakkara, M. Challacombe, P. M. W. Gill, B. Johnson, W. Chen, M. W. Wong, C. Gonzalez, J. A. Pople, *Gaussian 03, Revision C.02*, Gaussian, Inc., Pittsburgh, PA, **2003**.